JOURNAL OF PROPULSION AND POWER
Vol. 19, No. 5, September–October 2003

Multi-Element Unstructured Methodology for Analysis of Turbomachinery Systems

Vineet Ahuja,* Jeremy D. Shipman,† S. Arunajatesan,† and Ashvin Hosangadi‡
Combustion Research and Flow Technology, Inc., Pipersville, Pennsylvania 18947

In recent years unstructured mesh techniques have become popular for computational fluid dynamics analysis of external aerodynamic-type problems. The main advantages of such an approach include mesh generation over complex domains, grid adaptation in localized areas, and accuracy in efficiently identifying complexities in local flow physics. A hybrid unstructured methodology is used to carry out simulations for predominantly internal flow turbomachinery applications. Issues related to skewness and other constraints of tetrahedral meshes are addressed in the context of turbomachinery-based propulsive flows that exhibit a rich variety of length scales and timescales, as well as interesting flow physics. The unstructured framework permits the generation of a contiguous grid without internal boundaries between different components of a turbomachinery system and provides good local resolution in regions where the flow physics becomes important. The increased numerical stability resulting from these factors coupled with the parallel solution framework yields an efficient solution procedure for complex turbomachinery flows. Numerical results are presented and compared against experimental measurements for a transonic diffuser–volute configuration and a high Reynolds number pump.

Nomenclature

C_1, C_2	=	modeling constants in turbulent dissipation rate equation
$\boldsymbol{D}$	=	chemical turbulent source term
E	=	total internal energy per unit volume
$\boldsymbol{F}$	=	inviscid flux vector representing volumetric flux
f_1, f_2, f_μ	=	low Reynolds number empirical modeling functions
$\boldsymbol{G}$	=	viscous flux vector through each dual face
k	=	turbulent kinetic energy
N	=	normal dual vector area
n_x, n_y, n_z	=	components of normal duct vector area
P	=	pressure
$\boldsymbol{Q}$	=	vector of dependent variables
S_k, S_ε	=	source terms for turbulent kinetic-energy and turbulent dissipation rate equations resepctively
U	=	countervariant velocity along dual normal
U_r	=	velocity of control volume dual fare
u, v, w	=	velocity along coordinate directions
ε	=	turbulent dissipation rate
μ_T	=	turbulent viscosity
ρ	=	density
ρ_i	=	partial densities for chemical species
ρ_k	=	prediction term in turbulent kinetic energy equation

I. Introduction

TURBOMACHINERY plays a critical role in maintaining the efficiency of propulsion systems, heat pump systems, etc. Optimizing performance of the turbomachinery components associated with these systems such as impellers, diffusers, and volutes requires an accurate analysis of the complex physical phenomena such as secondary flows, blade–wake interaction, tip leakage, and cavitation. Furthermore, the coupling between the various components (multiple blade rows, inducer–impeller, and impeller–diffuser) can play an important role in improving/hampering efficiency of the system. For example, the inlet flow distortion from the impeller can feed into the diffuser–volute thereby changing the performance characteristics. Therefore, there is a push in the computational community toward developing generalized methodology for the concurrent analyses of the multiple components of the system.

The rapid evolution of parallel hardware technology has permitted the use of unstructured computational fluid dynamics (CFD) analysis as a viable option for large-scale computations of complex turbomachinery applications. Traditionally, unstructured methodology was developed for external aerodynamics-type problems. This led to the development of unstructured mesh generation algorithms, for example, advancing front[1,2] and Delaunay triangulation (see Refs. 3 and 4), that could very efficiently generate tetrahedral meshes for complex configurations such as entire aircraft. In particular, unstructured methodology allows for efficient grid generation of complex shapes that incorporate multi-component systems, where interfacing between the different components has traditionally been challenging for structured grid techniques. For instance, the cut-water or tongue region in a diffuser–volute configuration can be difficult to grid with a structured approach without either distorting the grid cells or introducing a singularity in the grid topology. Such a mesh can be easily generated utilizing an unstructured approach without any internal boundaries or skewed cells. Furthermore, grid adaptation can be readily used to improve the resolution locally in the mentioned cut-water or tongue region of a volute–diffuser and, thereby, the accuracy in localized regions of the flow domain where the flow physics dominates (pressurization and local flow acceleration in the tongue region).

The primary purpose of this paper is exploration of the unstructured grid philosophy in analysis of internal flow problems, particularly those associated with turbomachinery systems. Unlike problems in external aerodynamics, most turbomachinery systems are either confined by viscous boundaries, for example, blades, hub, shroud, diffuser walls, etc., or dominated by viscous phenomena, such as wakes shedding off blade surfaces. There are many challenges associated with the extension of the traditional unstructured methodology (tetrahedral cells) to turbomachinery-type problems: First, tetrahedral cells are very inefficient in resolving flow phenomena where the dominant physical phenomena exhibit gradients in one direction, for example, shear layers, wakes, plumes etc. The issues related to the degradation of accuracy of skewed triangular/tetrahedral elements have been discussed by Babushka and Aziz[5]

Received 5 August 2002; revision received 4 April 2003; accepted for publication 30 April 2003.

*Research Scientist, 6210 Keller's Church Road. Senior Member AIAA.
†Research Scientist. Member AIAA.
‡Principal Scientist. Member AIAA.

and have also been reported by Mavriplis.[6] For problems such as shear layers that exhibit directional gradients in the interior of computational domains, structured hexahedral elements offer an efficient alternative because these cells can be easily stretched to high aspect ratios to resolve the local physics in the dominant direction with little loss of accuracy. Tetrahedral cells, on the other hand, degrade in accuracy as they are distorted or skewed, and the reasonable way to resolve local gradients is by generating small near isotropic tetrahedral elements (with minimum distortion). This leads to the second challenge of maintaining a manageable size mesh while providing for sufficient resolution for resolving local phenomena. This problem is further exacerbated in certain turbomachinery geometries such as diffusers and volutes that are enclosed in viscous walls with severe topological constraints.

In this paper, we use a multi-element approach wherein an optimal use of tetrahedral, prismatic, pyramidal, and hexahedral cells are used to solve flows efficiently in complex turbomachinery systems. The motivation stems from the use of tetrahedral elements in resolving geometrical complexity, extrusion of prismatic layers from triangulated boundaries in resolving boundary-layer phenomena, and high aspect ratio hexahedral elements providing adequate clustering in local regions of high gradients, such as free shear layers and narrow viscous cross sections like those in diffusers. An example illustrating our point is shown in Figs. 1 and 2. Figure 1a shows the diffuser–volute geometry for which analyses will be carried out in the course of this paper. Two multi-element grids were generated for this diffuser-volute configuration. The first grid consists of a tetrahedral surface discretization with prismatic extrusion to resolve the boundary layers along the walls (Fig. 1b). The second strategy involves hexahedral discretization of the diffuser section with tetrahedral/prismatic discretization of the volute section (Figs. 2a and 2b).

The unstructured framework associated with analysis of multicomponent turbomachinery systems has been incorporated in the unstructured/multi-element solver called CRUNCH CFD. The CRUNCH CFD code[7–9] allows for solution of the Navier–Stokes equations on hybrid, multi-element unstructured meshes that include a combination of tetrahedral, prismatic, pyramid, and hexahedral cells. Because the algorithm utilized in the CRUNCH CFD framework is edge based, the flux computation is essentially grid transparent. No additional costs are accrued in the inviscid flux construction for the different elements that are used. Such an approach gives flexibility in gridding complex shapes or combinations of complex shapes with different elements without the computational costs associated with utilization of different elements, for example, cell-centered schemes. Computations are performed efficiently on parallel distributed computing platforms using message passing interface (MPI), and robustness is achieved through the use of implicit time-integration algorithms [gradual minimum residual (GMRES) and Gauss–Siedel)]. Convergence acceleration is achieved by the use of preconditioning methods.

Results are presented for a diffuser–volute configuration that is part of a centrifugal compressor onboard a ship air-conditioning system. The compressor was redesigned to use HCFC-124 refrigerant as a replacement to CFC-114, as part of a push toward environmentally friendly refrigerants. However the redesigned system underperformed relative to the design point, and detailed numerical simulations are being used to better understand these losses.[10,11] The inlet conditions to the diffuser comprise flow with a very high swirl velocity and a turbulent flowfield. The solution in this study was obtained with a hybrid prismatic-tetrahedral grid, where prismatic layers were put next to wall surfaces to resolve the boundary layer. Pressure profiles at various locations in the diffuser as well as on the volute surface compared well with experimental data. The numerical results have been analyzed to better understand the losses occurring in this configuration.

The second set of simulations pertains to a high Reynolds number pump. The pump consists of a 13-blade inlet guide vane (IGV) and a sweptback 7-bladed rotor with tip clearance. Detailed comparisons with experimental data are presented in this paper. This case is a good example of multiple blade rows simulations where complex flow phenomena such as blade–vortex interaction, tip vortex leakage, and flow separation are present. In the next section a brief overview of the numerical method is provided. This is followed by a discussion of the results for the diffuser-volute and the high Reynolds number pump and the comparisons with the experimental data. The last section summarizes our effort and conclusions that can be drawn from the application of multi-element methodology to the class of turbomachinery flows.

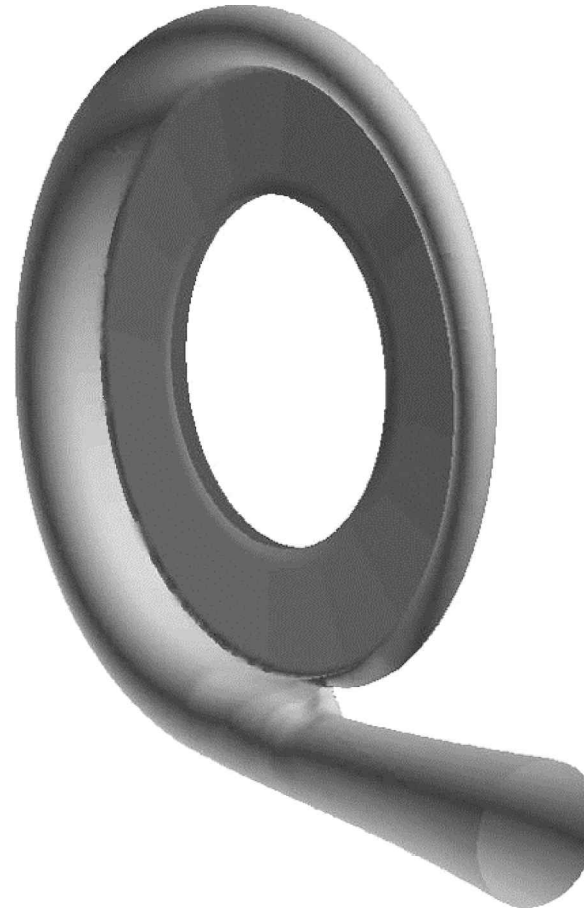

Fig. 1a Diffuser–volute configuration.

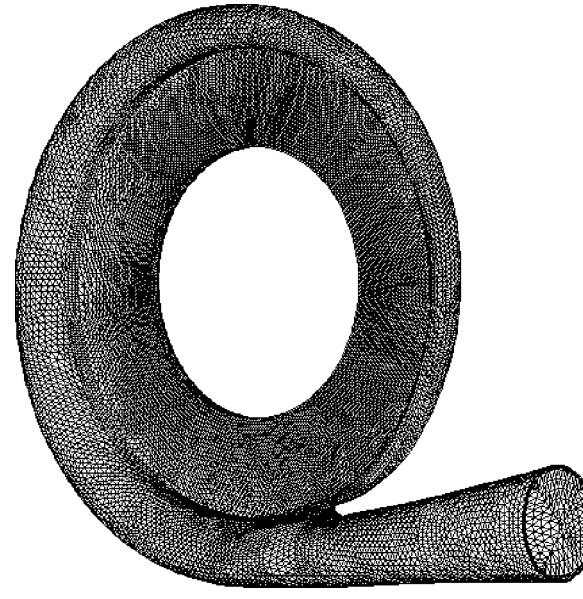

Fig. 1b Hybrid tetrahedral–prismatic contiguous grid for the diffuser–volute configuration.

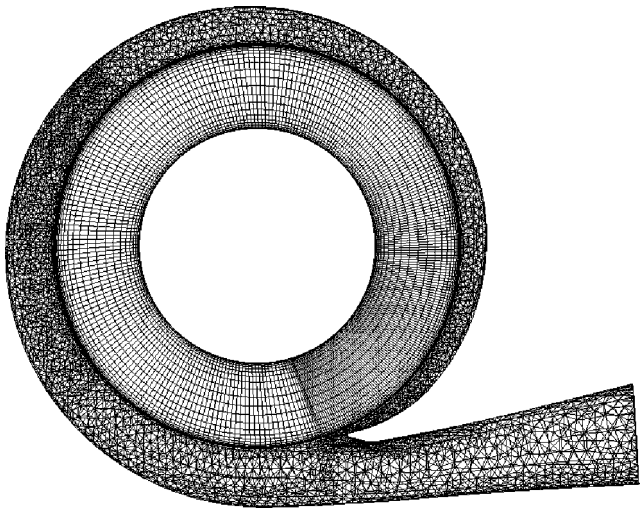

Fig. 2a Hybrid hexahedral–tetrahedral grid for diffuser–volute configuration.

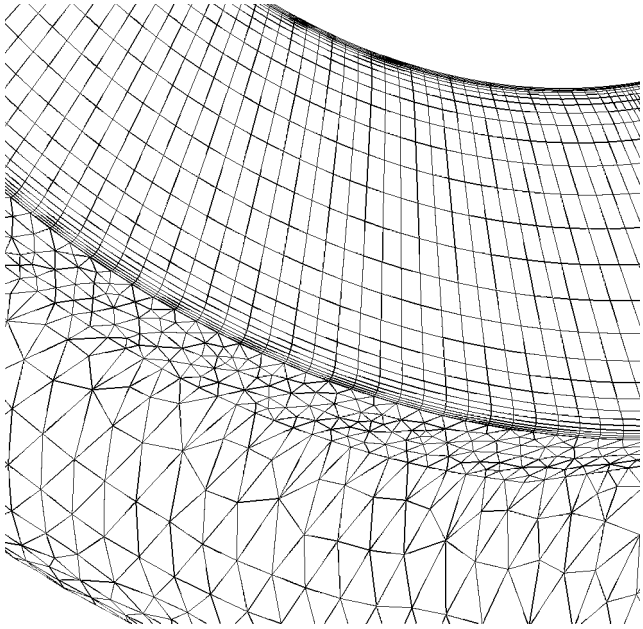

Fig. 2b Blowup of hexahedral–tetrahedral interface showing continuous grid along the diffuser–volute junction.

II. Numerical Method Overview

Equations and Basic Numerics

The CRUNCH CFD code[7–9] is a hybrid-element, that is tetrahedral, prismatic, pyramid, and hexahedral cells, unstructured flow solver for viscous, real gas systems, as well as multi-phase gas–liquid systems. It allows for generalized thermochemistry specification, permits dynamic grid motion, and has a coupled two-equation turbulence model. CRUNCH CFD is formulated for an edge-based data framework (following Barth[12,13]) where the solution is saved at the cell vertex and a dual control volume is defined by cutting across all edges coming to a node (Fig. 3).

Such an edge-based formulation is attractive when dealing with multi-elements because the dual surface associated with an edge can include contributions from different element types resulting in a grid transparent framework for inviscid flows. For efficient computation of large three-dimensional problems, a parallel framework for distributed memory systems has been implemented along with a sparse matrix (GMRES) solver,[9] thereby providing an advanced computational tool.

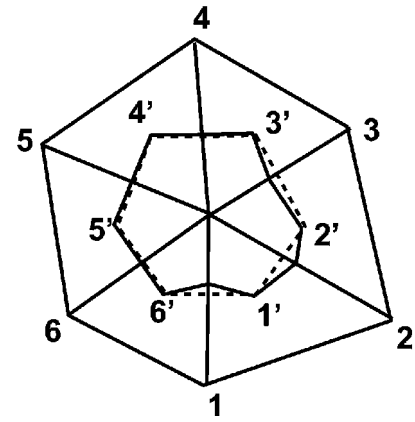

Fig. 3 Schematic indicating control volume and associated dual volume: ——, mesh; ——, median dual; and - - - -, centroid dual.

The governing equations are written in finite volume form for each vertex dual as follows:

$$\frac{\partial}{\partial t}\int_{\Omega} \boldsymbol{Q}\,\mathrm{d}V + \int_{\partial\Omega} \boldsymbol{F}(\boldsymbol{Q}, n)\,\mathrm{d}s = \int_{\partial\Omega} \boldsymbol{G}(\boldsymbol{Q}, n)\,\mathrm{d}s + \int_{\Omega} \boldsymbol{D}\,\mathrm{d}V \quad (1)$$

Following the standard notation, $\boldsymbol{Q}$ is the vector of dependent variables, $\boldsymbol{F}(\boldsymbol{Q}, n)$ is the inviscid flux vector, $\boldsymbol{G}(\boldsymbol{Q}, n)$ is the viscous flux vector, and $\boldsymbol{D}$ is the chemical/turbulent source term. The vectors $\boldsymbol{Q}$, $\boldsymbol{F}$, $\boldsymbol{G}$, and $\boldsymbol{D}$ are defined as

$$\boldsymbol{Q} = [\rho, \rho u, \rho v, \rho w, E, \rho_1, \ldots, \rho_s, \ldots, \rho_{\mathrm{NS}-1}, \rho k, \rho\varepsilon]^T \quad (2)$$

$$\boldsymbol{F}(\boldsymbol{Q}, n) = \begin{bmatrix} \rho(U - U_r) \\ \rho(U - U_r)u + n_x P \\ \rho(U - U_r)v + n_y P \\ \rho(U - U_r)w + n_z P \\ (E + P)U - EU_r \\ \rho_i(U - U_r) \\ \vdots \\ \rho_{\mathrm{NS}-1}(U - U_r) \\ \rho k(U - U_r) \\ \rho\varepsilon(U - U_r) \end{bmatrix} \quad (3)$$

A second-order linear reconstruction procedure (following Barth[12]) is employed to obtain a higher-order scheme. The higher-order variables need to be limited to yield a total variation diminishing scheme. We note that the inviscid flux procedure as outlined here is grid transparent; given a dual area associated with each edge the details of the different element types contributing to this edge are not relevant.

The viscous fluxes are computed by estimating the gradients (or stresses) at the cell faces and then performing a Green–Gauss integration of the stresses around each dual volume. (See Ref. 14 for details.) For hexahedral cells where the edge vectors are not skewed relative to the cell faces, an edge-based viscous flux procedure can be derived. However, for tetrahedral cells where edge skewness is substantial, the edge-based procedure fails, particularly for the k–ε equations, and is reflected in incorrect turbulent viscosity levels. For tetrahedral cells, a cell-based procedure has been implemented which that remedies this problem.

Turbulence Modeling

The standard high Reynolds number form of the k–ε equations forms the basis for turbulence modeling in CRUNCH. Transport equations for the turbulent kinetic energy and its dissipation rate are solved along with the basic momentum and energy equations. These equations, with supplemental low Reynolds number

Re terms, are

$$\frac{\partial \rho k}{\partial t} + \frac{\partial}{\partial x_i}\left[\rho u_i k - \left(\mu + \frac{\mu_T}{\sigma_k}\right)\frac{\partial k}{\partial x_i}\right] = P_k - \rho\varepsilon + S_k$$

$$\frac{\partial \rho \varepsilon}{\partial t} + \frac{\partial}{\partial x_i}\left[\rho u_i \varepsilon - \left(\mu + \frac{\mu_T}{\sigma_\varepsilon}\right)\frac{\partial \varepsilon}{\partial x_i}\right] = C_1 f_1 P_k - C_2 f_2 \rho\varepsilon + S_\varepsilon$$

$$\mu_T = C_\mu f_\mu \rho \frac{k^2}{\varepsilon} \tag{4}$$

where, σ_k, σ_ε, C_1, and C_2 are the modeling constants and f_1, f_2, and f_μ are low Reynolds number *Re* (near-wall) empirical modeling functions that equal unity in the high Reynolds number form.[15]

Solution Procedure: Parallel, Implicit Framework

For efficient computation of large three-dimensional problems, a parallel framework for distributed memory systems has been implemented along with an implicit solution procedure for the sparse implicit Jacobian matrix. The parallel framework is implemented by partitioning the grid into subdomains with each subdomain residing on an independent processor. Because the solution is solved for at the cell vertex, the control volume for the nodes lying on the interprocessor boundaries may span across processors. The net flux for the interprocessor nodes are obtained by summing up the fluxes computed independently on each processor, and hence, the explicit flux is identical to the single-processor solution.[14] The message passing between processors has been implemented using MPI to provide portability across various platforms.

The implicit solution procedure currently employs a GMRES solver with a preconditioning matrix using distance-one-neighbor bandwidth. Currently, the approximate Jacobian for the Roe-average flux is taken, and this together with the sparseness of the preconditioning matrix may affect the stability of the inversion procedure.

III. Simulation Results

Simulation of a Vaneless Diffuser-Volute System

We present results for a vaneless diffuser–volute configuration that is part of a 1.5 million Btu/h centrifugal compressor on a ship-based air-conditioning system. This compressor was redesigned to accept the environmentally friendly refrigerant HCFC-124. The compressor consists of two rows of IGVs, a vaneless diffuser, a volute, and its discharge diffuser. The radius ratio of the vaneless diffuser exit to the impeller exit is 1.52. The inlet width of the vaneless diffuser is 0.35 in., and the exit width is 0.1425 in. The compressor was tested at the Centrifugal Compressor Development Facility at the Annapolis Laboratory of the David Taylor Model Basin. A total of 40 static pressure taps were installed along the front plate and the back plate. They were distributed along the complete volute passage with a concentration of the pressure taps in the cut-water region.[5]

The measured performance of this compressor was found to be below the design specification. An analysis of the system component performance[5] indicates that the volute contains the largest area of loss in the compressor that results in the underperformance of the system. Hence detailed numerical studies have been carried out to better understand the causes of the losses in the volute. (Mavriplis[6] gives details on an earlier structured simulation for a similar configuration.)

In the present study, a tetrahedral–prismatic grid with approximately a million tetrahedral cells and 20,000 prismatic cells was generated. We observe that an unstructured approach alleviates some of the difficulties associated with structured grid generation for this problem. First, no internal periodic boundaries exist at the volute–diffuser interface, which is gridded through. Second, the cut-water region, which poses topological difficulties for the structured case, is handled easily here, and a high-resolution grid is obtained locally to resolve the high gradients expected in this region.

The flow conditions are transonic for this problem with the inflow to the diffuser having a Mach number of 1.0. The total velocity magnitude at the diffuser inflow is 128 m/s with the tangential component of the velocity accounting for 96% of this velocity magnitude. The temperature of the refrigerant is 302 K, and at this temperature the gamma has a low value of 1.12. The density of the refrigerant is 21.452 kg/m^3, and the Reynolds number of the flow is $3.17E+07$. Given the high swirl conditions and the transonic flow conditions, the boundary conditions become crucial in obtaining the correct results. In the present calculation, the inflow mass flux, stagnation temperature, and tangential velocity component were specified at the diffuser inlet, and a constant pressure was enforced at the volute exit. For the stagnation temperature and tangential velocity, a uniform profile was specified. Enforcing the mass flux boundary condition was found to be crucial in not generating pressure waves particularly because the swirl velocity has such a high value and yet does not contribute to the mass flux. We note that the calculation presented here was computed on 32 nodes of a CRAY T3E system using the GMRES procedure. The calculation took 12 h of wall clock time to converge.

The simulations show strong twisting action and vorticity generation in the volute. Consequently, there is an impetus to turbulence generation, which is reflected in the higher turbulent viscosity values at this location (Fig. 4). Thus, clearly, the shape of the volute cross section and the associated mixing losses from the flow turning from the diffuser are impacting the performance of the volute. In particular, conventional volute design theory that assumes uniform flow along the diffuser cross section is no longer valid.

The pressure contours (Fig. 5) show a smooth, fairly symmetrical pressurization as the fluid travels radially from the diffuser.

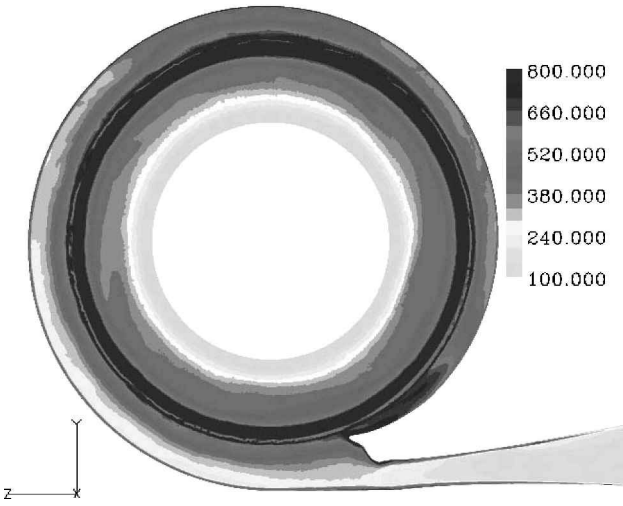

Fig. 4 Turbulent viscosity contours in diffuser–volute; turbulent viscosity levels plotted as a ratio of laminar viscosity.

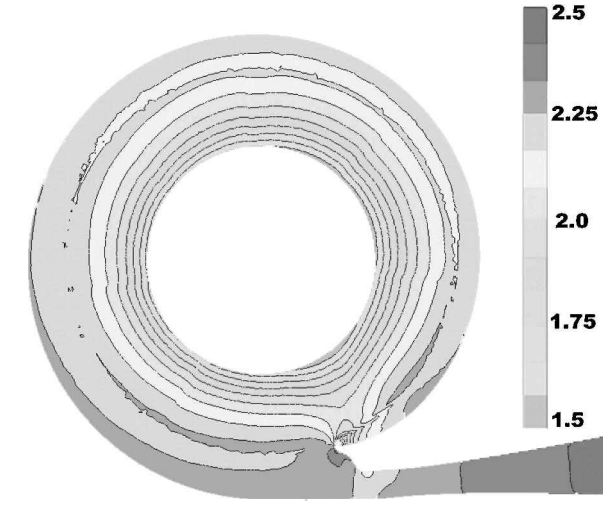

Fig. 5 Pressure contours along a cross section of the diffuser–volute system.

However, the cut-water region and the junction region of the discharge diffuser with the volute exhibit strong pressure variation. This region has a complex flow pattern with the following different streams of fluid interacting here: 1) fluid traveling along volute surface, 2) fluid coming directly from lower half of the diffuser, and 3) fluid coming through from the cutoff region. The confluence of these different streams imparts a swirl to the fluid as it enters into the discharge diffuser, which could potentially impact the design of the system downstream of this pipe.

The pressure profiles are plotted for two locations in the diffuser (radius of 1.12 and 1.52) in Fig. 6a and along the volute surface in Fig. 6b. Good comparisons are obtained at all three locations, which indicates that the flowfield is being predicted fairly well. In particular, the strong decrease in pressure at the cut-water region is predicted reasonably well. We note that this low-pressure region in the cut-water region affects the azimuthal pressure recovery along the diffuser and, hence, the overall performance of the system.

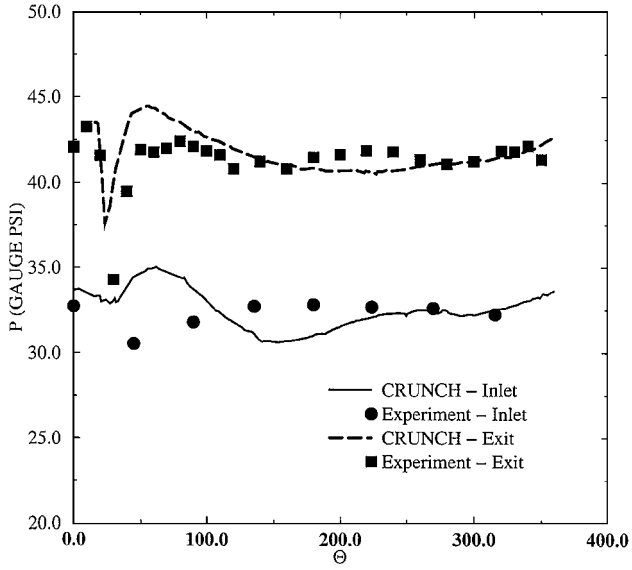

Fig. 6a Pressure comparisons of the simulations and experiments in the diffuser section at radius of 1.12 and 1.52.

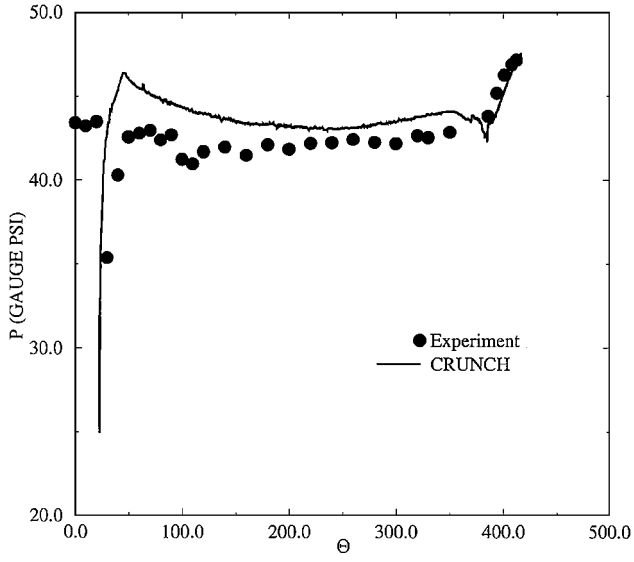

Fig. 6b Pressure comparisons of simulation and experiments on the surface of the volute.

Simulation of a High Reynolds Number Pump

Our next set of simulations pertain to a high Reynolds number pump that has a large body of detailed measurements and flow visualization data of the blade surfaces and the flowfield in the vicinity of the blade surfaces.[16,17] The pump consists of 13-blade IGV and a 7-blade backward swept rotor. The rotor rotates at 260 rpm and was tested in water at a Reynolds number of 2.3×10^6 based on the chord of the IGV blade. There exists a gap (equivalent to 2% of blade span) between the tip of the rotor and the outer casing that houses the pump. Simulations were first carried out on a hexahedral grid of a single IGV passage with periodic boundaries and on a multielement grid comprising of hexahedral, tetrahedral, and prismatic elements for the rotor.

The incompressible formulation of CRUNCH CFD[18] was utilized for this calculation with a two-equation k–ε turbulence model. Figure 7 shows the IGV geometry and pressure distribution over the IGV flow passages and on a planar cut along the midspan. A hexahedral grid with 250,000 elements was chosen for this simulation, primarily because of the simplicity of the blade profile and the IGV geometry (little variation in loading and no tip gap). Figure 8 shows a comparison of the predicted pressure with measured values at four different span locations extending from the hub to the tip. The profiles indicate good agreement with the

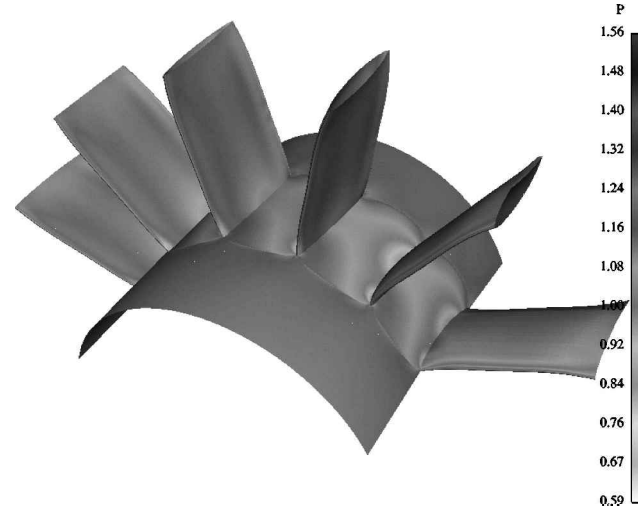

Fig. 7a IGV configuration with pressure distribution on blade surfaces.

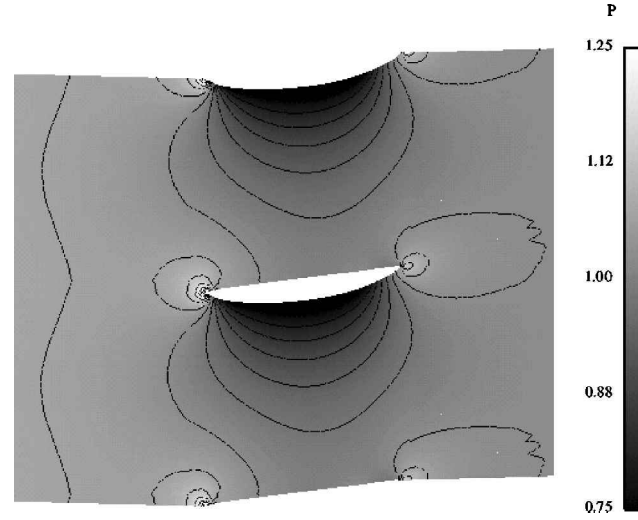

Fig. 7b Pressure distribution on midspan of the IGV, pressure scale normalized by $\rho_\infty u_\infty^2$ and freestream density of 996 kg/m^3 used with freestream velocity of 10.67 m/s.

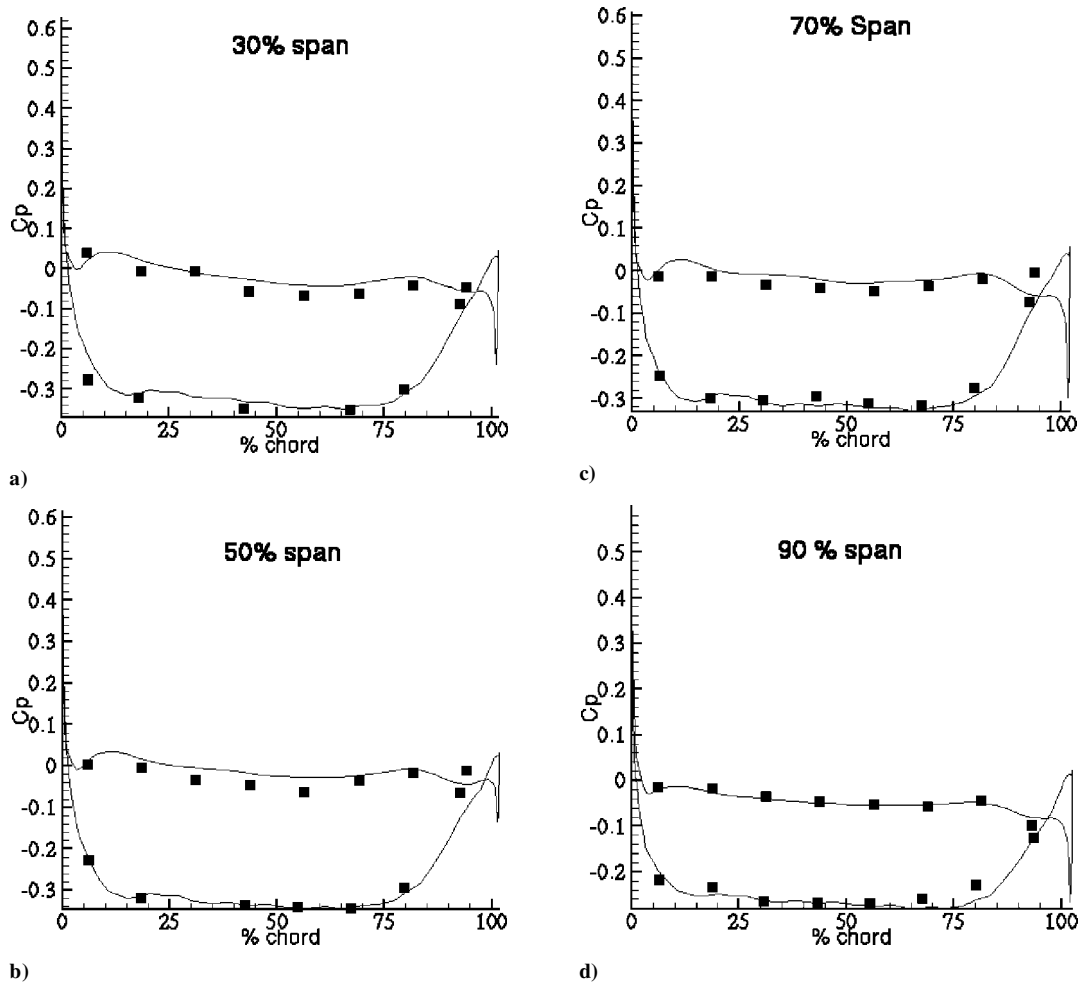

Fig. 8 Comparison of predicted pressure profiles with measured data on the stator blade surfaces.

measured data and show a steady decrease in loading from the hub to the tip. Close to the trailing edge, the suction pressure profiles at all span locations show an adverse pressure gradient. This corresponds to a small region of reverse flow near the trailing edge of the blade.

The rotor simulations were performed on a mixed element grid. A constant radial cut of the grid is shown in Fig. 9. The grid comprised 203,137 tetrahedral elements, 333,099 hexahedral elements, and 7956 pyramidal elements. The grid was tightly clustered in the tip gap region and in regions close to the blade surface, hub, and shroud with hexahedral elements. Because of the large spacing between the IGV and the rotor, a mixing plane was determined between the IGV and the rotor, and the IGV solution (pressure, axial, radial, and tangential components of velocity) was circumferentially averaged and imposed as a boundary condition for the rotor. This ensured a radial distribution of the flow variables from the IGV solution served as an inflow condition for the rotor, a condition sufficient to procure a steady solution for the rotor.

The pressure predictions on the rotor blade surfaces (Figs. 10a and 10b) are compared against measured data at various span locations in Fig. 11. Again, the predicted profiles indicate excellent agreement with the measured data. The pressure profiles show the same trends in loading that were observed earlier for the stator blades. However, the loading on the rotor blades is significantly greater than that was seen in the case of the IGV. This is to be expected because the rotor blades are responsible for work done by the pump on the fluid.

The most interesting phenomenon related to this particular pump is the existence of a tip vortex due to the gap between the rotor blades and the shroud. The pressure difference due to the blade

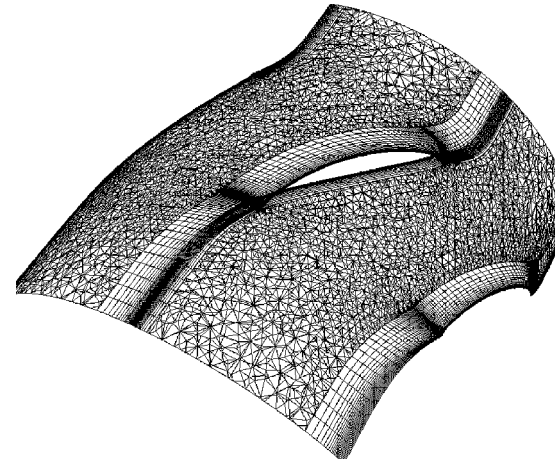

Fig. 9 Multi-element grid for the rotor: constant radius cut showing hexahedral region used to capture gradients in the boundary layer with tetrahedral cells between blade rows.

loading and the relative motion between the blade and the outer shroud contribute to the formation of a tip-leakage vortex on the suction side of the blade. The tip-leakage vortex migrates circumferentially close to the shroud in a direction opposing the motion of the blade rotation. This produces substantial losses that reduce pump efficiency and leads to the onset of cavitation due to the low pressure in the vortex core. The tip vortex in our simulations is indicated in Fig. 12, where a surface of constant radius close to the blade

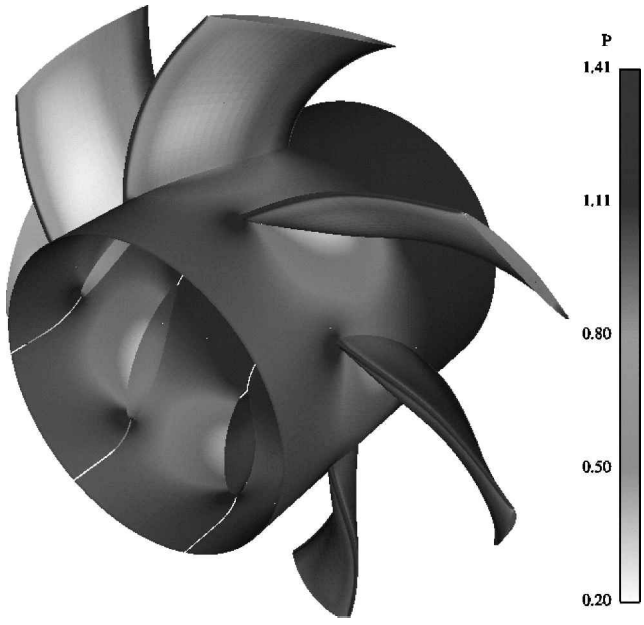

Fig. 10a Rotor configuration with pressure distribution on blade surfaces.

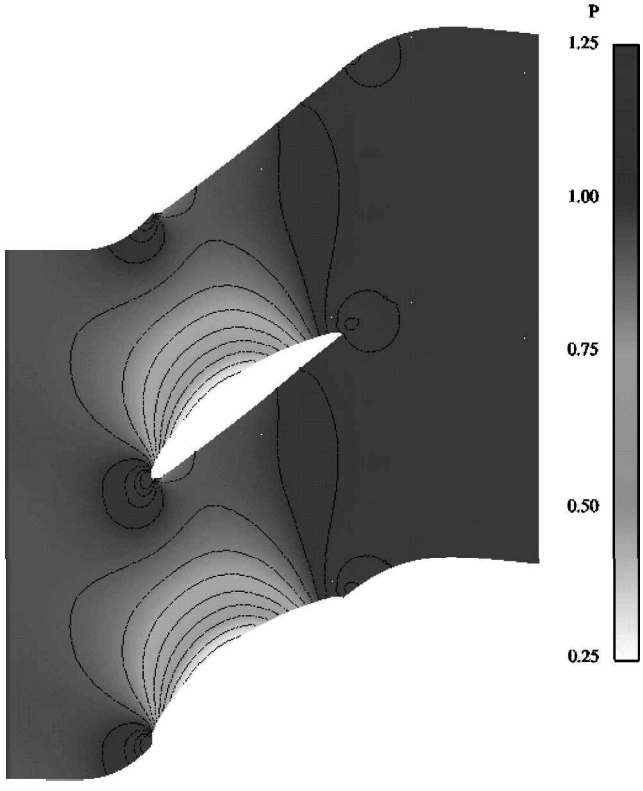

Fig. 10b Pressure distribution near midspan of the rotor; pressure scale normalized by $\rho_\infty u_\infty^2$ and freestream density of 996 kg/m^3 used with freestream velocity of 10.67 m/s.

top is shown. In Fig. 12, levels of turbulent viscosity are shown that correspond to vorticity and the path of the tip vortex. Note that the grid resolution deteriorates rather rapidly between the blades. This is mostly because the trajectory of the tip vortex is not known a priori, and subsequent simulations can be carried out with grid refinement along this trajectory. As mentioned earlier, the pressure in the vortex core falls below the vapor pressure leading to the formation of cavitating zones.[18] Further investigation needs to be carried out to capture accurately the pressure drop and cavitation associated with the tip vortex.

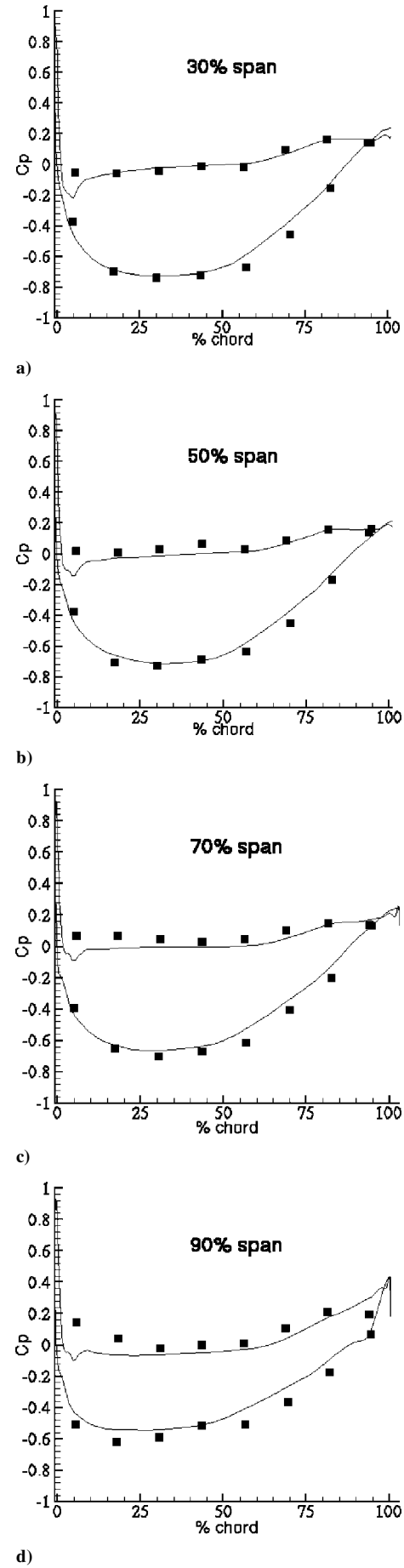

Fig. 11 Comparison of predicted pressure profiles with measured data on rotor blade surfaces.

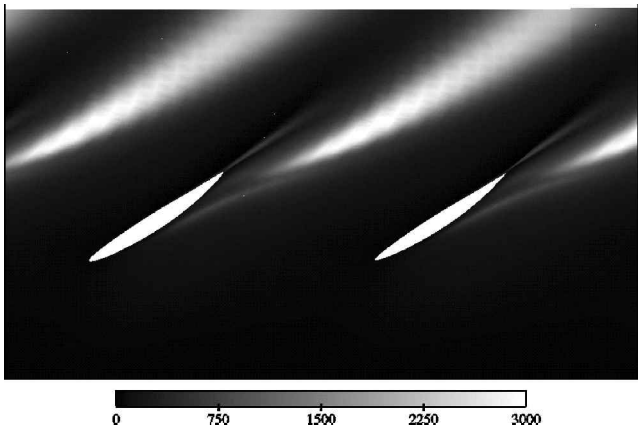

Fig. 12 Turbulent viscosity distribution, with tip vortex location on a surface of constant radius close to the blade tip; turbulent viscosity levels normalized by molecular viscosity of 8×10^{-4} (N · s)/m^2.

IV. Conclusions

The features of a multi-element unstructured methodology have been demonstrated for a variety of turbomachine applications ranging from transonic compressors to incompressible axial pumps. The simulated results are in good agreement with measured data and reported experimental observations. Furthermore, the multi-element framework gives increased flexibility in grid generation for complex configurations that are routinely found in turbomachinery systems. Because the local grid topology may be tailored for the flow requirements, accurate solutions may be obtained with economical grid sizes by embedding tetrahedral cells while providing adequate resolution of local phenomena such as blade wakes, secondary flow, and blade–wake interaction with high aspect ratio hexahedral cells. The combination of a parallel framework with domain decomposition strategies and implicit sparse matrix solvers results in a very efficient numerical scheme for large three-dimensional applications that are the hallmark of most turbomachinery systems.

Acknowledgments

The authors would like to thank Yu-Tai Lee of David Taylor Model Basin for technical discussions and his help during the course of this work.

References

[1]Pirzadeh, S., "Three-Dimensional Unstructured Viscous Grids by the Advancing Layers Method," *AIAA Journal*, Vol. 34, No. 1, 1996, pp. 43–49.

[2]Lohner, R., and Parikh, P., "Generation of Three-Dimensional Unstructured Grids by the Advancing Front Method," *International Journal for Numerical Methods in Fluids*, Vol. 8, 1988, pp. 1135–1149.

[3]Baker, T. J., "Three-Dimensional Mesh Generation by Triangulation of Arbitrary Point Sets," *Proceedings of 8th AIAA CFD Conference*, Honolulu, June 1987, pp. 255–271.

[4]Baker, T. J., "Unstructured Meshes and Surface Fidelity for Complex Shapes," *Proceedings of 10th AIAA CFD Conference*, AIAA, Washington, DC, 1991, pp. 714–725.

[5]Babushka, I., and Aziz, A. K., "On the Angle Condition in the Finite-Element Method," *SIAM Journal on Numerical Analysis*, Vol. 13, No. 2, 1976, pp. 214–226.

[6]Mavriplis, D. J., "Unstructured Grid Techniques," *Annual Review of Fluid Mechanics*, Vol. 29, 1997, pp. 473–514.

[7]Hosangadi, A., Lee, R. A., York, B. J., Sinha, N., and Dash, S. M., "Upwind Unstructured Scheme for Three-Dimensional Combusting Flows," *Journal of Propulsion and Power*, Vol. 12, No. 3, 1996, pp. 494–503.

[8]Hosangadi, A., Lee, R. A., Cavallo, P. A., Sinha, N., and York, B. J., "Hybrid, Viscous, Unstructured Mesh Solver for Propulsive Applications," *AIAA 34th Joint Propulsion Conference*, AIAA Paper 98-3153, Cleveland, OH, July 1998.

[9]Hosangadi, A., Cavallo, P. A., Arunajatesan, S., Ungewitter, R., and Lee, R. A., "Aero-Propulsive Jet Interaction Simulations Using Hybrid Unstructured Meshes," *35th AIAA/ASME/SAE/ASEE Joint Propulsion Conference and Exhibit*, AIAA Paper 99-2219, Los Angeles, CA, June 1999.

[10]Bein, T. W., and Lee, Y.-T., "Performance Evaluation of an Air-Conditioning Compressor Part I: Measurement and Design Modeling," *International Journal of Rotating Machinery*, Vol. 5, No. 4, 1999, pp. 231–240.

[11]Lee, Y.-T., and Bein, T. W., "Performance Evaluation of an Air-Conditioning Compressor Part II: Volute Flow Predictions," *International Journal of Rotating Machinery*, Vol. 5, No. 4, 1999, pp. 241–250.

[12]Barth, T. J., "A 3-D Upwind Euler Solver for Unstructured Meshes," *Proceedings of 10th AIAA CFD Conference*, Washington, D.C., June 1991, pp. 228–238.

[13]Barth, T. J., "Numerical Aspects of Computing Viscous High Reynolds Number Flows on Unstructured Meshes," *29th AIAA Aerospace Sciences Meeting and Exhibit*, AIAA Paper 91-0721, Reno, NV, Jan. 1991.

[14]Barth, T. J., and Linton, S. W., "An Unstructured Mesh Newton Solution for Compressible Fluid Flow and Its Parallel Implementation," *33rd AIAA Aerospace Sciences Meeting and Exhibit*, AIAA Paper 95-0221, Reno, NV, Jan. 1995.

[15]Papp, J. L., and Dash, S. M., "Turbulence Model Unification and Assessment for High-Speed Aeropropulsive Flows," *39th AIAA Aerospace Sciences Meeting and Exhibit*, AIAA Paper 2001-0880, Reno, NV, Jan. 2001.

[16]Zierke, W. C., Farrell, K., and Straka, W. A., "Measurement of the Tip Clearance Flow for a High Reynolds Number Axial-Flow Rotor: Part I—Flow Visualization," American Society of Mechanical Engineers, *International Gas Turbine and Aeroengine Congress and Exposition*, ASME Paper 94-GT-453, The Hague, Netherlands, June 1994.

[17]Zierke, W. C., Farrell, K., and Straka, W. A., "Measurement of the Tip Clearance Flow for a High Reynolds Number Axial-Flow Rotor: Part II—Detailed Flow Measurements," American Society of Mechanical Engineers, *International Gas Turbine and Aeroengine Congress and Exposition*, ASME Paper 94-GT-454, The Hague, Netherlands, June 1994.

[18]Ahuja, V., Hosangadi, A., and Arunajatesan, S., "Simulations of Cavitating Flows Using Hybrid Unstructured Meshes," *Journal of Fluids Engineering*, Vol. 123, No. 2, June 2001, pp. 331–340.